Published in final edited form as:
J Am Chem Soc. 2010 May 5; 132(17): 6081–6090. doi:10.1021/ja909850s.

High Resolution Spectral Analysis of Individual SERS-Active Nanoparticles in Flow

Gregory Goddard[†], **Leif O. Brown**[‡], **Robb Habbersett**[†], **Christina I. Brady**[‡], **John C. Martin**[†], **Steven W. Graves**[§], **James P. Freyer**[†], and **Stephen K. Doorn**[*,‡]

[†]National Flow Cytometry Resource, Bioscience Division, Los Alamos National Laboratory, Los Alamos, NM 87545

[‡]Chemistry Division, Los Alamos National Laboratory, Los Alamos, NM 87545

[§]Center for Biomedical Engineering, Department of Chemical and Nuclear Engineering, University of New Mexico, Albuquerque, NM 87131

Abstract

Nanoparticle spectroscopic tags based on surface enhanced Raman scattering (SERS) are playing an increasingly important role in bioassay and imaging applications. The ability to rapidly characterize large populations of such tags spectroscopically in a high-throughput flow-based platform will open new areas for their application and provide new tools for advancing their development. We demonstrate here a high resolution spectral flow cytometer capable of acquiring Raman spectra of individual SERS-tags at flow rates of hundreds of particles per second, while maintaining the spectral resolution required to make full use of the detailed information encoded in the Raman signature for advanced multiplexing needs. The approach allows multiple optical parameters to be acquired simultaneously over thousands of individual nanoparticle tags. Characteristics such as tag size, brightness, and spectral uniformity are correlated on a per-particle basis. The tags evaluated here display highly uniform spectral signatures, but with greater variability in brightness. Subpopulations in SERS response, not apparent in ensemble measurements, are also shown to exist. Relating tag variability to synthesis parameters makes flow-based spectral characterization a powerful tool for advancing particle development through its ability to provide rapid feedback on strategies aimed at constraining desired tag properties. Evidence for single tag signal saturation at high excitation power densities is also shown, suggesting a role for high-throughput investigation of fundamental properties of the SERS-tags as well.

Introduction

Recent interest in the application of surface enhanced Raman scattering (SERS) to flow cytometry[1,2] has been spurred by the potential use of SERS in novel optical tags for bioassay and imaging applications.[3-12] Flow cytometry is a powerful and versatile approach to high throughput analysis, finding widespread use in clinical diagnostics, fundamental biochemical studies, and the development of pathogen detection and drug discovery applications.[13] Currently, flow cytometry approaches to cell marker analysis, immunoassays, evaluation of molecular avidity, etc. are typically assessed primarily by fluorescence labeling and readout. The introduction of multi-color flow cytometry has allowed simultaneous multi-analyte assays and multiple parameter measurements to be performed on individual cells in a sample stream.[14] This enhanced capability drives a

[*]To whom correspondence should be addressed. skdoorn@lanl.gov

continuing demand to further expand the number of distinct measurements made on each cell, with a concurrent interest in high resolution instrument development.[15-25] However, the degree of spectral overlap between the various fluorophores limits simultaneous multiparameter measurement, and has led to interest in alternate, non-fluorescent, probes.[2,26,27]

One such alternative involves the use of Raman-based probes. Fluorescence spectra are typically broad and featureless, with emission peak widths in the range of 50 – 60 nm. Furthermore, multi-color applications require multiple excitation and detection channels. In contrast, Raman probes generate highly featured fingerprint spectra consisting of many narrow lines (typically <0.5 nm FWHM), allowing multiple overlapping spectra from different molecules to be easily distinguished, with the further advantage of reducing the instrumentation requirements to include only single source excitation and a single detector. Thus, Raman-based optical probes are inherently suitable for advanced multiplexed analysis. While the use of intrinsic Raman is made difficult by small Raman cross sections, SERS can provide more than sufficient sensitivity based on scattering by 'tags' consisting of Raman-active molecules adsorbed on nanostructured gold or silver surfaces.[7,28,29] In principle, many types of nanostructures can be employed as SERS-tags, including stabilized colloidal particles,[7,28,29] nanoshells,[30,31] and small nanoparticle aggregates.[32-35] The large variety of potentially suitable tag structures has led to a surge in research related to their application in assays and imaging. In flow cytometry applications, individual SERS-tags may serve to both identify and signal the presence of an analyte or the occurrence of a binding event of interest and may also serve as the foundation for encoded capture beads.[36]

In short, SERS-based detection offers the opportunity to significantly advance in-flow multiplexing. The resultant technique presents a unique potential for ultra-sensitive molecular identification and analysis. However, while many of the fundamental building blocks are now available, there remain significant challenges to realizing in-flow Raman-based multiplexing. Its full exploitation requires effective full spectral data acquisition, which can only be achieved once several interlinked objectives are met. The instrumentation must possess sufficient sensitivity to both capture single nanoparticle SERS-tag spectra and yield the spectral resolution required to allow detailed analysis of all information encoded in a spectrum. Yet this sensitivity must be achieved with rapid analysis times (particles typically transit a flow cytometer's laser in ~10 μs) in order to provide the high throughput demanded of flow cytometry. This, in turn, requires SERS-tags that are optimized both in terms of spectral brightness, and spectral diversity.

Despite the availability of many potential tag architectures, coupled with an understanding of key factors contributing to SERS signal strength and quality, the ability to batch engineer suitable structures with quantitative and consistent properties remains elusive. This is critical since flow cytometry examines individual tags, and not ensemble properties. Tag-to-tag variability typically includes differences in absolute signal intensity, which will limit applicability to quantitative assays. Peak-to-peak variations within the spectral signature, and features such as changing background intensities, may also disrupt fingerprint patterns. Fidelity must be preserved in these spectral signatures across all tags in a population to maintain confidence in the ability to use the fingerprint features to identify all targeted species in a given assay. Possible contributions to this behavior come from variations in dye loading between tags, as well as from differences in molecular orientation of the bound dyes, which may be due to either chemical or electrostatic variations between binding sites. Additionally, impurity species or photodegradation products from unstable dyes may contribute new features. Beyond chemical binding effects, factors determining the plasmonic response of the nanoparticle architectures also impact variability. These include existence of a size distribution for individual nanoparticles and differences in the relative

dimensions of core and shell in multi-component particles. In the case of SERS-tags based on small nanoparticle aggregates, differences in the number of constituent particles and relative aggregation geometries determine the extent of electromagnetic “hot-spots” generated from interparticle interactions. Such geometric factors may also feed back into chemical effects such as different electrostatic behavior at dye binding sites. One recent development addressing this issue takes the approach of first self-assembling polymer-stabilized dimers and small clusters, followed by infusion of the SERS-active molecule.[37]

To the extent that these contributions to variability in SERS-tag response are controllable synthetically, improvements in SERS-tag synthesis will require a reliable method to obtain quantitative, statistically significant data addressing questions of SERS signal uniformity in ensembles of purportedly identically fabricated SERS substrates. In particular, rapid characterization of individual nanoparticle SERS-tags is required for direct evaluation of particle-to-particle variability. Ideally, such characterization will provide simultaneous correlated multi-parameter measurements of optical and geometric characteristics directly tied to SERS-tag performance, including fully-resolved spectral fingerprints, SERS brightness, and Rayleigh scattering efficiency. The results can be linked to specific preparation conditions to guide future synthesis. Such single-particle evaluation would also be invaluable in providing a meaningful direct comparison of the different nanostructures currently being developed as SERS-tags. Measurements at the single particle level also provide fundamental insight into intrinsic behaviors impacting SERS response (such as particle-dependent plasmon damping[38,39]) that are often masked at the ensemble level. Beyond the clear impact such rapid measurements would have on further enabling of the broad range of SERS-tag applications, similar issues related to property variability are also important for a variety of nanostructured materials used in electronic and optical applications.

Current characterization methods for SERS-active nanoparticles are inefficient, normally interrogating immobilized particles one by one via single mode optical, electron, and/or scanning probe microscopies. Most studies present data for only a small number (typically not more than ~100) of nanoparticles, providing limited statistics for addressing issues of synthetic uniformity. Correlation of separate measurements on selected particles typically requires spatially registered sample deposition and serial application of the various measurement techniques. While these methods have provided important fundamental information, the lengthy data acquisition impedes useful feedback into particle development. Reliance on such static samples can also skew statistics by acquiring the combined responses of overlapping particles. While there are faster techniques for morphological characterization, such as dynamic light scattering, they produce at best a skewed average size and lack the ability to perform multiparameter measurements on the per particle basis needed for correlating SERS signal to the size and structure of a SERS-tag.

Recently, Laurence et al[40] presented a method that represents a major step forward in solving these analysis problems. This work extends fluorescence[23] and Raman correlation spectroscopies[41,42] to investigate the scattering characteristics of solution-based SERS-tags diffusing through a confocal laser spectrometer. Histograms can be generated that correlate individual SERS-tag size, polarization response, Raman, Rayleigh, and continuum backgrounds for thousands of tags. While providing powerful information in a short time, the approach has two key unaddressed issues: (a) Detection is performed at only two wavelengths, allowing correlation of SERS intensity to background and scattering rates, but providing no evaluation of the uniformity of spectral signatures. (b) Analysis rates are limited by diffusion, while diffusing particles can theoretically pass through the beam multiple times resulting in potentially skewed statistics. One approach to addressing the latter issue is to perform the measurements in flow.[1,2,43]

We present here the successful convergence of two significant objectives, representing the realization of both high-throughput Raman-based multiplexed analysis and a method for the rapid nanoparticle characterization required to meet the needs of SERS-tag development. We describe a flow cytometer capable of Raman signal acquisition in analytically relevant rates required of current fluorescence-based cytometers. Instrument sensitivity allows collection of the full Raman fingerprint region with a 14 μs particle residence time. Furthermore, instrument sensitivity is attained without the need to bin data pixels in frequency space to artificially boost signal intensity, thus maintaining the highest possible spectral resolution. Significantly, this permits full access to the high information content encoded within the SERS-tag spectrum, while enabling assessment of the variability of not just tag brightness, but also fidelity of the spectral signature. Additionally, we demonstrate the capability of this instrument to obtain correlated multiparameter measurements on individual SERS-tags, which are used to characterize SERS-tag populations. The SERS signatures of several different tag types are evaluated over thousands of particles to correlate brightness and spectral variability with background and scattering behavior. Certain preparations show relative standard deviations in spectral response as low as 5%. In more variable populations, the correlated information provides clear discrimination between subpopulations of tags generated within a single preparation batch. We thus demonstrate an approach that enables both the quantitative statistical evaluation of SERS signal uniformity based on synthesis conditions and evaluation of SERS nanoparticles for use in cytometry. Furthermore, the flexibility of the resulting capability will be of general interest for extension to direct comparisons of competing SERS-tag architectures, exploration of a range of fundamental properties of plasmonic particles, and application to other nanoparticle types.

Experimental

Synthesis and Characterization of SERS-Tags

SERS-tags were prepared as previously described.[34] Aqueous silver nanoparticles were prepared by reduction of silver nitrate using sodium citrate.[44] The size distribution of the silver cores was found to be 67 ± 17 nm by analysis of TEM images (JEOL 3000F) using ImageJ software.[45] Conditions for coating the nanoparticles vary somewhat for different dyes, and between particle batches. As a generic example, 3-mercaptopropyltrimethoxysilane (MPTMS, 750 μL, 25 μM) was added to silver nanoparticles (15 mL, 1.1×10^{-10} M) with vigorous stirring for 45 s. At this point, the desired dye (50 – 200 μL (mL Ag)$^{-1}$, 2.8 μM) was introduced with continued stirring. Aggregation was then induced by the addition of sodium chloride (50 – 180 μL (mL particles)$^{-1}$, 1%). After further mixing for 6 min, sodium silicate (1,800 μL, 0.54%) was added to begin the glass coating process. After six days, the excess sodium silicate was removed by centrifuging the solution three times (14,500 × *g*, 25 min), replacing the supernatant with water each time. Final SERS-tag concentrations are estimated at 10^8 particles per mL. The bulk SERS spectra of the nanoparticles were obtained with a Kaiser Optical fiber optically-coupled probehead spectrometer using 0.5 mW of excitation at 514.5 nm or 488 nm.

Full-Spectral Raman Flow Cytometer

Complete details of the Raman flow instrumentation are given in Supporting Information. Briefly, the system is constructed around a BD FACSCalibur flow chamber and emission/light scatter collection optics (Figure 1a). The sample stream is delivered through a quartz flow chamber at 10 μL min^{-1}. A sheath stream (3 mL min^{-1}) of phosphate buffered saline (PBS) concentrically envelopes and hydrodynamically focuses[46] the sample stream to a core diameter of approximately 15 μm. Approximately 14 μs particle transit times result. Crossed cylindrical lenses are used to focus 50 mW of excitation light at 514.5 or 488 nm from an

argon ion laser into the sample as an ellipse approximately 50 μm wide by 12 μm high. Raman emission is collected via a high numerical aperture (N.A. of 1.1) lens and focused into an f/2.2 spectrograph, which spectrally disperses the light along the long axis of a high efficiency, low-noise, electron-multiplied CCD array detector (EMCCD, 1600 × 200 pixels). A cross section of the flow cell is imaged vertically on the detector, with the central sample stream covering 30% of the CCD height. Pixels within this central 30% are binned vertically on-chip, providing sufficient sensitivity that additional binning in the horizontal (frequency) direction is not required to further boost signal strength. The full spectral resolution capability of the 1600 pixel dimension is thus maintained.

Data acquisition is triggered using forward (FSC) and side scattering (SSC) (Fig. 1a) signals obtained from a photomultiplier tube (PMT) or photodiode, respectively. Scatter signals are independently excited at 532 nm by a solid state laser spatially separated from the Raman excitation source (Fig. 1b). Scatter signals are collected through a locally developed miniature data acquisition system (MICAS).[47] The EMCCD data are saved in CSV file format and subsequently exported into MATLAB for analysis. Simultaneously acquired background spectra (see Supporting Information) are subtracted from the sample spectra to remove background Rayleigh scatter from the flow chamber and Raman scatter from water.

A schematic of a second flow cytometer optimized for sensitivity, but limited to filter-based cytometric measurement of a broad spectral window, is shown in Fig. 1c. The flow cell and sample delivery for this high-sensitivity instrument has been described in detail previously.[24] Laser excitation (1-3 mW) at 532 nm is focused to a ~ 10 μm spot onto the sample stream inside a 250-μm square cross-section flow channel. Rayleigh scatter is detected via a PMT, while the SERS signals are collected with an avalanche photodiode (APD). Full details of the custom data acquisition system (ORCAS) used to collect data from this instrument are described in a separate publication.[25]

Results and Discussion

High Throughput Single SERS-tag Spectroscopy

Flow cytometers are uniquely designed for rapid parameterization and sorting of individual microscopic particles within large populations suspended in a stream of fluid. Particles in a hydrodynamically focused stream are passed through the intersection of an excitation/probe laser and optical collection region. Various detectors may be incorporated for collection of forward and side light scatter (FSC and SSC, respectively, in Figure 1a), and detectors for fluorescence or (as introduced here) Raman emission. Each particle passing the laser scatters light in proportion to its size and shape, and bound fluorescent or Raman-active tags are excited into emission. The capture of light scatter correlated with these Stokes-shifted signals enables quantitative multiparametric analysis of the physical or chemical properties of single particles at rates as high as 50,000 per second. While conventional flow cytometers achieve this at specific wavelengths using combinations of dichroic mirrors and filters, the technique is shifting to implementations of grating or prism dispersion onto array detectors, enabling full spectral detection in flow designs that can be modified to detect SERS.[1,2,16,21,24]

We have designed our system around a commercial flow-cytometry platform. This provides a generally accessible approach to nanoparticle characterization that will facilitate broad use. A key aspect to enhancing all aspects of system performance has been the optimization of the fluidic behavior via differential pressure and volumetric control of the flow streams. The result is a minimized sample interrogation volume and extremely stable flow conditions. This is critical for providing the uniform particle trajectories and probe transit times required to limit the impact of diffusion, which can be significant for the nanoscale particles of

interest.[40] Such stable trajectories now allow direct triggering off of scatter from the small (~100 nm) tag particles, and also enable the precise timing required to exactly match gating of signal acquisition to the residence time of a SERS-tag in the probe volume. When paired with tightly focused excitation and high numerical aperture collection optics that probe only the core sampling volume, remarkable sensitivity results from significant overall suppression of background. The high system performance is rounded out by the low noise and high gain characteristics of the EMCCD.

To act as a true single SERS-tag analyzer, particle coincidence rates must be minimized. At higher concentrations, multiple SERS-tags were observed to pass through the interrogation volume during a single CCD exposure. To reach acceptable limits, our as-produced SERS-tags were diluted 1000-fold with PBS (final concentration of ~10^5 particles mL^{-1}) to generate passage rates of about 10 per second. As analysis rates reach this limit, scattering intensities are observed to decrease in a stepwise manner, allowing particle triplets, doublets, and true singlets to be distinguished (see Supporting Information). An upper bound may then be set on the triggering threshold to discriminate against particle multiplets. Furthermore, given a camera exposure of 20 μs per frame, and random tag arrival dictated by Poisson statistics, at our analysis rates the probability of measuring more than one SERS-tag in a given spectrum is approximately 2×10^{-5} % and the probability of more than one particle passing through the interrogation region anytime during readout is less than 0.08%.[48] While conservatively low concentrations were used for these experiments to guarantee single-particle analyses, it is clear that significantly higher event rates could be used. Furthermore, higher digitization rates on the CCD would allow even higher analysis rates without coincidence by tradeoff between flow rate versus digitization noise. Finally, for quantitative purposes, missed particles must also be minimized. We estimate a loss rate < 0.1%, achievable both due to the stable sample flow and by acquiring data well within the limiting readout rate of the EMCCD (1000 s^{-1}). One obvious additional benefit of the flow-based characterization is that particles are only measured once.

While many SERS-tag architectures exist, we use tags based on controlled aggregation of Ag nanoparticles[34] to demonstrate our flow-based single nanoparticle spectroscopy. These provide a convenient source of bright tags, from a synthesis process that permits easy incorporation of a wide range of dye molecules as the source of our spectral signatures. Examples of ensemble spectra obtained from three different SERS-tag types are shown in Figure 2a. These tags display a widely varying array of narrow spectral features that allow the easy discrimination of tag signatures from each other.

In comparison, representative spectra, captured in flow, from corresponding single tag particles are shown in Figure 2b. The ability for full-spectral acquisition, at single SERS-tag sensitivities, in applications-relevant acquisition times (20 μs) is thus demonstrated. Furthermore, these high-quality single tag spectra are obtained at the lowest gain setting of the EMCCD. Sufficient dynamic range remains available for evaluation of significantly less-bright particle types. The single tag spectra are found to compare well to the bulk spectra. Excellent resolution is observed between closely spaced peaks and even weaker features are seen to be retained.

These observations demonstrate the important link between sensitivity and limiting spectral resolution. The two work together to preserve the observable tag signature. With appropriate instrument design it is not necessary to trade resolution for gains in sensitivity (through binning in frequency space, for example). For the tags displayed here, this is especially important for resolving spectral differences in the highly featured region between 1200 and 1700 cm^{-1}. Ultimately, such simultaneous gains in sensitivity and resolution allow for the

use of a greater number of tag combinations in multiplexed assays and the development of more complex spectral signatures.

We show spectra obtained both at 514 nm and 488 nm excitation to further demonstrate versatility in the choice of excitation wavelength. We have also obtained similar results with 532 nm and 647 nm excitation. Use of a full range of commonly used laser lines is readily incorporated via matching of the appropriate optical filters to the excitation source. Excitation wavelength can then be envisioned as another multiplex dimension by pairing with the matching resonance behavior of select SERS-tags.

Spectral Variability in SERS-Tag Response

The ability to obtain high quality spectra in flow at the single SERS-tag level now allows a ready evaluation of the variability in the SERS-tag response from particle to particle over large populations of individual tags. Figure 3 shows stacked spectra acquired from 1000 individual particles for the three different tag species discussed for Figure 2. This representation of the data provides a rapid qualitative visual assessment of the spectral variability (including both frequency and intensity factors) for a broad range of individual particles. The different tag types illustrate the range of behavior that may be observed. The oxazine 170 tags (Figure 3a) show significant uniformity over the entire sampled population, while the response for styryl 9M (Figure 3b) and safranine (Figure 3c) tags exhibit more variability, primarily as changes in their background signals.

These results highlight the ability to obtain direct comparisons of response between different tag types, on a *per particle basis*, that overcomes difficulties with obtaining meaningful comparisons from bulk suspensions. Such comparisons in bulk may be limited by differences in particle concentration, tag architectures and composition, among other factors. Perhaps the biggest factor represented in the ensemble spectra is they are blind to the occurrence of subpopulations in SERS response. One extreme example may be that the observed spectra may originate from a small population of extremely bright particles, while the bulk of the ensemble may display a very weak response. For the tags sampled in Figure 3a this is not the case, with no spectrally “dead” particles being observed. The tags sampled in Figure 3c, however, suggest that other types of subpopulations do occur in our samples, such as the group of spectra showing a discontinuous jump in background intensity in the safranine case.

Of particular interest for multiplexing applications is the degree of variability present in the overall spectral signatures. Variability may manifest itself as large changes in relative intensities between spectral features and by the occurrence of spurious peaks present for select tags. However, inspection of the spectra shown in Figure 3 suggests that good stability in the spectral signatures for all tag species is possible. These issues can be evaluated more quantitatively through direct correlation of the spectral behavior to other particle characteristics.

One measure of the spectral uniformity is to evaluate the percent standard deviation (%SD) of the spectral response obtained at each frequency pixel over each 1000-tag sampling. The results for the three tag species under investigation are shown in Figure 4. The %SDs in the spectral signature are found to range from 1% to 8%, averaging about 4%. Interestingly, the spikes in the %SD for each tag directly correspond to their specific Raman peaks. No significant fluctuations are observed at other frequency locations, indicating that spurious peaks unrelated to the bulk tag signatures do not occur for these populations. At a more fundamental level, these results indicate a stability in dye binding geometries and resistance to photochemical degradation in the SERS tags. The broad feature at low frequencies in

Figure 4 for styryl 9M arises from a more significant variation in background in this part of the spectrum, likely resulting from variability in particle geometries (see below).

In addition to using the raw %SD values, spectral variability can be evaluated by correlating changes in peak intensities to fluctuations in background response for several different frequency ranges. It is also useful to correlate fluctuations between specific peaks as well. Figures 5a and 5b show how peak SERS intensities for several features from two different dye systems (oxazine 170 and safranine) correlate to fluctuations in their nearby background regions. Low frequency and continuum background features common to SERS spectra can originate both from the Ag substrate and ionic adsorbates.[49-51] Thus, background fluctuation can come from ionic impurities and is also likely correlated to the degree of aggregation for each of the nanoparticle aggregates. Our own characterization by TEM has shown a wide size distribution in the nanoparticle aggregates used in this work.[34] Fluorescence background may also be present, originating from dye species trapped in the SiO_2 coating layer but not bound at the Ag surface. We see that the variability in the SERS response for the safranine peaks evaluated in Figure 5b appears strongly correlated to the background fluctuations, indicating that much of the background variability likely originates in the differences between various aggregate geometries, which will also strongly impact SERS response. More uncorrelated variability, such as found in the oxazine case (Figure 5a) could then likely be minimized through improvement in quality control parameters aimed at better impurity rejection and improved rinsing of particles prior to glass coating in the synthesis process.

In addition to understanding how peak intensities correlate to background fluctuations, how intensity changes at one peak correlate to those at other peaks is critical to determining the variability present in a given spectral signature. In Figure 5c we show how the intensities of two safranine peaks (at 598 and 1541 cm^{-1}) correlate to each other. We find strong correlation between the two peak intensities. A strong (or weak) response at 598 cm^{-1} is accompanied by a matching response at 1541 cm^{-1}. There are no anti-correlated cases in which a weak response at one peak is matched to a strong response for the other. These results are further evidence of stable spectral signatures over all sampled particles. The intensity response of the spectrum behaves the same across the entire frequency range, thus preserving the relative intensities of all features. This finding is in agreement with our previous work, which showed that small populations of tags bound to support beads give identical spectral signatures from one bead to the next.[36] The results shown here-demonstrate such spectral stability for the first time at the *single-tag* level.

Taken together, the data in Figures 5a and 5b also provide evidence that small subpopulations of behavior do occur in SERS-tag ensembles. For example, a subpopulation of tags experiencing increased background levels, in the presence of stable safranine SERS response, is clearly indicated in Figure 5b. This subpopulation corresponds to the spectra in Figure 3c that discontinuously jump to higher overall intensity. There also appears to be a subpopulation of tags in the oxazine 170 sample (Figure 5a) with lower intensities at the 1638 cm^{-1} peak, while high frequency backgrounds remain stable. These contrasting behaviors further demonstrate that factors leading to spectral and background variability will not necessarily always be coupled. Access to such detailed information highlights the importance of the full spectral detection capability we demonstrate here, especially regarding the ability to evaluate the suitability of tag populations for providing stable identifying signatures.

Intensity Variability in SERS-Tag Response

While stable spectral signatures are essential for encoding applications of the SERS-tags, uniformity in their intensity is required for quantitative applications. In order to develop

improved synthetic approaches aimed at uniform intensity response, it is also of interest to understand how variability correlates with factors like particle geometry and size. Such information can be extracted from plots of SERS intensity versus Rayleigh scatter for a given population. While this information is available from the full-spectral data sets discussed above, the total intensity response can be more efficiently evaluated by simultaneously collecting signal over the full frequency band of the SERS spectrum. To this end, we have also evaluated our SERS-tag characteristics on a second high-sensitivity flow cytometer (Figure 1c). The bandpass filter incorporated in this instrument's SERS detection channel effectively allows signal integration over all SERS bands occurring in the highly featured region between 1100 cm^{-1} and 1700 cm^{-1}. By utilizing PMT and APD detectors for this purpose, Rayleigh and Raman scattering intensities can be evaluated in real time. Such real-time evaluation of particle responses allows the high-sensitivity instrument to serve as a platform for further particle manipulation, while also providing statistics on a larger number of particles than is available with the full-spectral measurements.

In Figure 6 we show correlated SERS and Rayleigh scattering intensities obtained for each of the three dye tags discussed above. Each of the bivariate histograms incorporates data for approximately 10,000 individual SERS-tags. For comparison, we show in Figure 6a data from a commercial sample of 100-nm diameter polychromatic fluorescent nanospheres from Polysciences (of similar size to the SERS-tags). The fluorescent tags display tightly spaced responses for both emission and side-scatter intensities, indicating a highly monodisperse population in both size and fluorescence intensity, typical of what is required for quantitative flow cytometry applications. A significantly broader range of behaviors is found in the SERS-tags. While SERS intensities for the styryl 9M and safranine tags (Figure 6c and 6d) approach the uniformity displayed by the fluorescent tags, the oxazine 170 tags (Figure 6b) have significantly more variability. Despite this, we note that in all cases the SERS-tags are typically an order of magnitude brighter than the fluorescence tags, giving a direct demonstration of their potential to complement fluorescence-based approaches to flow-based multiplexing.

To first order, the magnitude of side-scatter for each particle can be taken as a relative measure of its size. The spread in side-scatter for all SERS-tags is found to be an order of magnitude larger than that for the fluorescent tags, indicating significant variability in aggregate sizes resulting from only limited control over the aggregation process in the tag synthesis.[34] It is interesting to note that the oxazine 170 SERS intensities are reasonably correlated to particle size, while those for styryl 9M and safranine appear relatively insensitive to size. This may be indicative of some degree of intensity dependence on the influence different dyes may have on the aggregation process, and the varying aggregation geometries that may result. Previous studies have shown that the organic dyes incorporated in the SERS-tags will themselves induce some degree of aggregation.[32,34] Different dyes were found to have varying effectiveness, which is not yet well understood. The ability to now evaluate multiple spectral parameters in flow may provide a useful tool for further exploration and understanding of this behavior.

The high-sensitivity cytometer is also useful for examining batch-to-batch variability in tag preparation and to compare the properties of labeled versus unlabelled SERS tags. Figure 7a shows a bivariate histogram for a set of unlabeled Ag aggregate particles. These show a similar variability in side-scatter/particle size as the preparations giving the results of Figure 6, and also display a low level of intrinsic Raman background signal. Results for a separate preparation of safranine-labeled tags are shown in Figure 7b and show, unsurprisingly, that labeled aggregates give much higher signal intensities. However, the correlated SERS versus Rayleigh signals in this tag set clearly separate into two ranges of behavior, with approximately 10% of the tags giving only a background response similar to the unlabeled

aggregates of Figure 7a. This result provides unambiguous evidence of two distinct subpopulations of particles occurring for this sample. In this particular safranine tag batch, a lower level of dye loading was tested. It is possible that under such conditions, some nanoparticle aggregates possess insufficient insertion of dyes into hot spots for strong SERS signal generation, resulting in the negligible response of the lower population shown in Figure 7b.

The higher excitation power densities and longer laser/particle interaction time available with the high-sensitivity instrument allow us to observe an additional interesting fundamental behavior for the brightest set of SERS-tags examined (safranine-labeled tags, Figure 6d). In Figure 6d we note that the top of the cluster of dots indicating the population of SERS-tags shows a flat top. This behavior is typically indicative of saturation when seen in fluorescence signals, and may indicate here that even as the aggregates get larger, there is no further SERS signal increase. Measurement of a set of extremely bright fluorescent ImmunoCheck microspheres (Beckman-Coulter, Fullerton, CA), revealed that the saturation level for the SERS-tags was at least two orders of magnitude lower than the signal saturation limit for the detectors or data acquisition system.

To explore this effect more closely, we examined the safranine-labeled SERS-tags at several different power levels (see Figure 8). A univariate histogram of side scatter for ~8000 particles (Figure 8a), shows that as excitation power is increased from 1 mW to 1.5 mW, and then 3mW, scatter signals increase linearly, as expected. However, the behavior of the SERS signal response differs significantly (Figure 8b). As incident power increases, so does the SERS response, but only to a point. We find that at the highest powers only the lower intensity particles in the population continue to get brighter (move to the right), leading to an asymmetric shape in the histogram where the right hand side has a rapid drop off. This behavior is mirrored in the bivariate histograms that correlate side scatter with SERS signal for the 1 mW and 3 mW cases (Figures 8c and 8d, respectively). Increasing power uniformly shifts the entire particle population to higher scattering intensities and maintains the observed breadth in the distribution. In contrast, maximum SERS intensities are found to saturate at higher powers, but the lower intensity particles observed at 1 mW excitation are found to shift into the higher intensity population, thus narrowing the observed intensity spread at higher powers. This signal saturation could be due to a number of effects, including: loss of dye due to desorption or photobleaching at the higher cycling rates, reorganization of the nanoparticle aggregate structure, nonlinear effects driven by higher power densities and plasmon field enhancements, and others. Further investigation is required to obtain a better understanding of this behavior.

It is interesting to note that the saturation of the single SERS-tag response contrasts with the highly linear behavior of the SERS-tag intensities found over several orders of magnitude of excitation power in ensemble measurements.[52,53] Ensemble measurements are typically performed at much lower power densities than applied in the high-sensitivity instrument. However, this contrasting behavior may also be resolved by recognizing that the results of Figures 8c and 8d show that dimmer particles are continuously moved into the brighter, saturated population as power is increased, thus the overall ensemble response also continues to increase. Total saturation of the ensemble response will not occur until all particles in a given sampling volume become individually saturated. These results again highlight the importance of interrogating the SERS-tag response on a single particle basis; fundamental behaviors masked in the ensemble become apparent at the single-tag level. From a practical perspective, this interesting fundamental behavior might ultimately be exploited by incorporating high power density excitation into the full-spectral instrument. The resulting signal saturation could be used to significantly narrow the observed variability in SERS intensities.

Conclusion

We have presented an efficient and highly sensitive flow-based approach to high-throughput, high-resolution spectral analysis capable of characterizing single nanoparticle SERS-tags on a per particle basis. Optimized optics, detectors, and fluidics incorporated into a conventional flow cytometry platform support full-spectral Raman analysis and multiparameter characterization capability with data acquisition times (20 μs) relevant to real-world assay requirements. The ability to simultaneously evaluate such parameters as Rayleigh scattering and SERS intensities and saturation power levels over multiple excitation wavelengths allows us to address various characterization issues essential to advancing SERS-tag applications, including variability in SERS-tag size, structure, spectral signatures, and brightness that may lead to the occurrence of significant subpopulations of tag performance. This capability has allowed us to demonstrate that SERS-tags can match and even exceed the brightness of fluorescent tags, while maintaining highly stable spectral signatures. Paired with the spectral flow cytometry capability, Raman-based tagging approaches are now poised to be incorporated into advanced multiplexed assay applications previously dominated by fluorescent tags. A range of new applications involving the interrogation of individual multiplexed cells or capture beads, in which multiple species of SERS-tags are simultaneously bound at different receptor sites and evaluated on a single particle, is now possible. The ability to collect the entire Raman spectrum at high spectral resolution with single tag sensitivity is critical to enabling such future assays. Access to well-resolved spectra with high information content permits the use of standard mathematical deconvolution techniques to extract individual tag spectral signatures from a multiplexed signal while maintaining quantitative intensity information.

Beyond enabling multiplexed in-flow assay applications, our approach to single-nanoparticle spectroscopy is envisioned as a powerful new tool both for advancing the development of a variety of nanoparticle systems and also for high-throughput probing of their fundamental properties. This unique capability will be invaluable for correlating multiple SERS-tag properties (brightness, signature, geometry) to production parameters to provide rapid feedback for improving and tuning synthesis conditions to yield SERS-tags with pre-designed and uniform properties. One aspect of such tag optimization is selection of the most appropriate nanoparticle architectures to incorporate into the tags. To this end, we will apply the spectral flow capability as an ideal platform for direct comparison of competing nanoparticle types (single colloid, nanoshell, and core-shell particles; nanostars; dimers; and various aggregate approaches) that will also help to address the fundamental debate over their comparative properties in a meaningful way. The potential also exists for multiparameter optical evaluation of other nanoparticle types (e.g., quantum dots, nanowires, nanotubes).

Additionally, as our spectral and high sensitivity instruments are flow cytometers, and provide the ability to actively evaluate optical signatures in real-time, it should be possible to sort selected SERS-tags based on optical parameters of interest similar to conventional flow cytometric sorting.[46,54] Such a sorting capability can be used to isolate the brightest particles within an ensemble into a single uniform population for later application as monodisperse tags. By separating a tag sample into specific subpopulations, the fundamental origins of their different SERS responses can also be probed by correlating their optical behavior to physical and morphological properties through subsequent analysis of individual subpopulations by electron and scanning probe microscopies and nephelometry. The in-flow spectroscopy capability also provides new opportunities for exploring other fundamental behaviors, including the SERS signal saturation represented in Figure 8, and dye-particle interactions. Further geometrical characterization of the SERS-tags can also be provided by incorporating additional optical probes, including both nonlinear spectroscopies[55-57] and

dynamical polarization measurements,[40] into the high-sensitivity measurement platform to take advantage of the slower flow rates it provides.

Supplementary Material

Refer to Web version on PubMed Central for supplementary material.

Acknowledgments

The authors thank Dr. Jessica Houston for many helpful discussions. This research was supported by LANL Laboratory Directed Research and Development funds and the National Flow Cytometry Resource (NIH Grant RR-01315).

References

(1). Watson DA, Gaskill DF, Brown LO, Doorn SK, Nolan JP. Cytometry A 2009;75A:460–464. [PubMed: 19199345]

(2). Watson DA, Brown LO, Gaskill DF, Naivar M, Graves SW, Doorn SK, Nolan JP. Cytometry A 2008;73A:119–128. [PubMed: 18189283]

(3). Cao YC, Jin R, Mirkin CA. Science 2002;297:1536–1540. [PubMed: 12202825]

(4). Graham D, Thompson DG, Smith WE, Faulds K. Nat. Nanotech 2008;3:548–551.

(5). Wabuyele MB, Vo-Dinh T. Anal. Chem 2005;77:7810–7815. [PubMed: 16316192]

(6). Qian X, Peng X-H, Ansari DO, Yin-Goen Q, Chen GZ, Shin DM, Yang L, Young AN, Wang MD, Nie S. Nat. Biotech 2008;26:83–90.

(7). Ni J, Lipert RJ, Dawson GB, Porter MD. Anal. Chem 1999;71:4903–4908. [PubMed: 10565281]

(8). Jun B-H, Kim J-H, Park H, Kim J-S, Yu K-N, Lee S-M, Choi H, Kwak S-Y, Kim Y-K, Jeong DH, Cho M-H, Lee Y-S. J. Comb. Chem 2007;9:237–244. [PubMed: 17298100]

(9). Sun L, et al. Nano Lett 2007;7:351–356. [PubMed: 17298000]

(10). Vo-Dinh T, Kasili P, Wabuyele M. Nanomedicine 2006;2:22–30. [PubMed: 17292112]

(11). Zavaleta CL, Smith BR, Walton I, Doering W, Davis G, Shojaei B, Natan MJ, Gambhir SS. Proc. Natl. Acad. Sci 2009;106:13511–13516. [PubMed: 19666578]

(12). Nowak-Lovato KL, Rector KD. Appl. Spectrosc 2009;63:387–395. [PubMed: 19366503]

(13). Sklar LA, Edwards BS, Graves SW, Nolan JP, Prossnitz ER. Ann. Rev. Biophys. Biomol. Struct 2002;31:97–119. [PubMed: 11988464]

(14). Roederer M, Brenchley JM, Betts MR, De Rosa SC. Clin. Immunol 2004;110:199–205. [PubMed: 15047198]

(15). Isailovic D, Li H-W, Phillips GJ, Yeung ES. Appl. Spectrosc 2005;59:221–226. [PubMed: 15720763]

(16). Wade CG, Rhyne RH Jr. Woodruff WH, Bloch DP, Bartholomew JC. J. Histochem. Cytochem 1979;27:1049–1052. [PubMed: 110874]

(17). Basiji D, Ortyn WE, George TC, Brawley J, Hall BE, Morrissey P. Cytometry A 2004;59A:87.

(18). Gauci MR, Vesey G, Narai J, Veal D, Williams KL, Piper JA. Cytometry 1996;25:388–393. [PubMed: 8946147]

(19). Robinson JP. Biophotonics Int 2004;11:36–40.

(20). Fuller RR, Sweedler JV. Cytometry 1996;25:144–155. [PubMed: 8891444]

(21). Dubelaar GBJ, Gerritzen PL, Beeker AER, Jonker RR, Tangen K. Cytometry 1999;37:247–254. [PubMed: 10547609]

(22). Jett J, Albright K, Graves S, Habbersett R, Martin J, Naivar M, Parson J, Wilder M, Yoshida T. Cytom. Suppl 2002:142–146.

(23). Goddard G, Martin JC, Naivar M, Goodwin PM, Graves SW, Habbersett R, Nolan JP, Jett JH. Cytometry A 2006;69A:842–851. [PubMed: 16969803]

(24). Habbersett RC, Jett JH. Cytometry A 2004;60A:125–134. [PubMed: 15290713]

(25). Naivar MA, Parson JD, Wilder ME, Habbersett RC, Edwards BS, Sklar L, Nolan JP, Graves SW, Martin JC, Jett JH, Freyer JP. Cytometry A 2007;71A:915–924. [PubMed: 17680705]

(26). Jaiswal JK, Goldman ER, Mattoussi H, Simon SM. Nat. Methods 2004;1:73–78. [PubMed: 16138413]

(27). Kaul Z, Yaguchi T, Harada JI, Ikeda Y, Hirano T, Chiura HX, Kaul SC, Wadhwa R. Biochem. Cell Biol 2007;85:133–140. [PubMed: 17464353]

(28). Doering WE, Nie S. Anal. Chem 2003;75:6171–6176. [PubMed: 14615997]

(29). Mulvaney SP, Musick MD, Keating CD, Natan MJ. Langmuir 2003;19:4784–4790.

(30). Levin CS, Kundu J, Barhoumi A, Halas NJ. Analyst 2009;134:1745–1750. [PubMed: 19684894]

(31). Jensen RA, Sherin J, Emory SR. Appl. Spectrosc 2007;61:832–838. [PubMed: 17716401]

(32). Su X, Zhang J, Sun L, Koo T-W, Chan S, Sundararajan N, Yamakawa M, Berlin AA. Nano Lett 2005;5:49–54. [PubMed: 15792411]

(33). Brown LO, Doorn SK. Langmuir 2008;24:2178–2185. [PubMed: 18220434]

(34). Brown LO, Doorn SK. Langmuir 2008;24:2277–2280. [PubMed: 18278969]

(35). McCabe AF, Eliasson C, Prasath RA, Hernandez-Santana A, Stevenson L, Apple I, Cormack PAG, Graham D, Smith WE, Corish P, Lipscomb SJ, Holland ER, Prince PD. Farad. Disc 2006;132:303–308.

(36). Brady CI, Mack NH, Brown LO, Doorn SK. Anal. Chem 2009;81:7181–7188. [PubMed: 19670884]

(37). Braun GB, Lee SJ, Laurence T, Fera N, Fabris L, Bazan GC, Moskovits M, Reich NO. J. Phys. Chem. C 2009;113:13622–13629.

(38). Baida H, Billaud P, Marhaba S, Christofilos D, Cottancin E, Crut A, Lermé J, Maioli P, Pellarin M, Broyer M, Del Fatti N, Vallée F, Sánchez-Iglesias A, Pastoriza-Santos I, Liz-Marzán LM. Nano Lett 2009;9:3463–3469. [PubMed: 19719148]

(39). Nehl CL, Grady NK, Goodrich GP, Tam F, Halas NJ, Hafner JH. Nano Lett 2004;4:2355–2359.

(40). Laurence TA, Braun G, Talley C, Schwartzberg A, Moskovits M, Reich N, Huser T. J. Am. Chem. Soc 2009;131:162–169. [PubMed: 19063599]

(41). Schrof W, Klinger JF, Rozouvan S, Horn D. Phys. Rev. E 1998;57:R2523–R2526.

(42). Eggeling C, Schaffer J, Seidel CAM, Korte J, Brehm G, Schneider S, Schrof W. J. Phys. Chem. A 2001;105:3673–3679.

(43). Sebba DS, Watson DA, Nolan JP. ACS Nano 2009;3:1477–1484. [PubMed: 19472989]

(44). Lee PC, Meisel D. J. Phys. Chem 1982;86:3391–3395.

(45). [Accessed 9/10/2009]. Available online from NIH at http://rsb.info.nih.gov/ij/

(46). Shapiro, HM. Practical Flow Cytometry. Wiley; Hoboken, NJ: 2003. p. 142-150.

(47). Naivar MA, Wilder ME, Habbersett RC, Woods TA, Sebba DS, Nolan JP, Graves SW. Cytometry A 2009;75A:979–989. [PubMed: 19852060]

(48). Keij JF, van Rotterdam A, Groenewegen AC, Stokdijk W, Visser JWM. Cytometry 1991;12:398–404. [PubMed: 1935455]

(49). Jiang J, Bosnick K, Maillard M, Brus L. J. Phys. Chem. B 2003;107:9964–9972.

(50). Otto A, Timper J, Billmann J, Kovacs G, Pockrand I. Surf. Sci 1980;92:L55–L57.

(51). Heritage JP, Bergman JG, Pinczuk A, Worlock JM. Chem. Phys. Lett 1979;67:229–232.

(52). Brown, LO. unpublished results

(53). Bello JM, Stokes DL, Vo-Dinh T. Anal. Chem 1989;61:1779–1783.

(54). Albright, KL.; Cram, LS.; Martin, JC. In: Kompala, DS.; Todd, P., editors. Cell Separation Science and Technology; ACS Symposium Series 464; American Chemical Society; Washington, DC. p. 73-78.

(55). Lippitz M, van Dijk MA. Orrit, M. Nano Lett 2005;5:799–802.

(56). Jin RC, Jureller JE, Kim HY, Scherer NF. J. Am. Chem. Soc 2005;127:12482–12483. [PubMed: 16144383]

(57). Palomba S, Danckwerts M, Novotny L. J. Optics A 2009;11:114030.

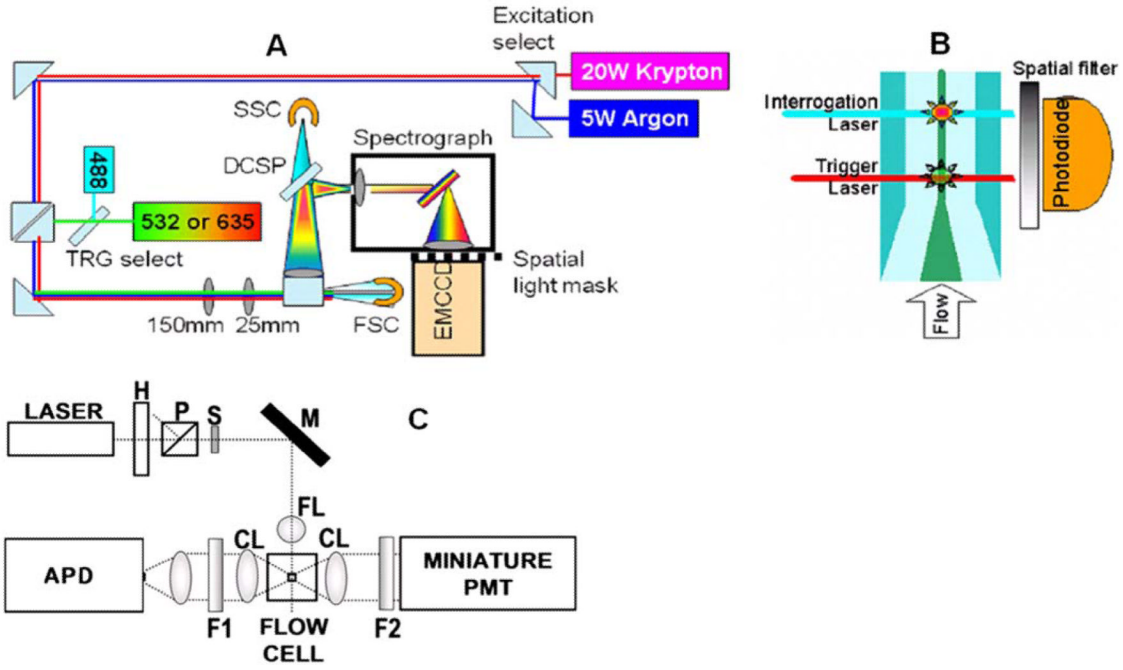

Figure 1.

(a) Top-view schematic of Raman full-spectral flow cytometer experimental apparatus with grating-spectrograph dispersive element. Flip mirrors are used to allow selection of krypton or argon laser excitation and 488 nm or diode laser (532 or 635 nm) for the trigger (TRG) laser. DCSP: dichroic short pass filter, SSC: side scatter PMT detector, FSC: forward scatter photodiode detector. (b) Sideview schematic of flow cell showing spatial separation of trigger and interrogation lasers. Sample stream (dark central region) is hydrodynamically focused by the surrounding sheath flow (lighter colored region). (c) Diagram of the high-sensitivity cytometer optics breadboard, flow cell, and sample holder. H, half wave plate; P, polarizer; S, shutter; M, mirror; FL, focusing lens; CL, collection lens; F1, filter 1; F2, filter 2; PMT photomultiplier tube and APD avalanche photodiode.

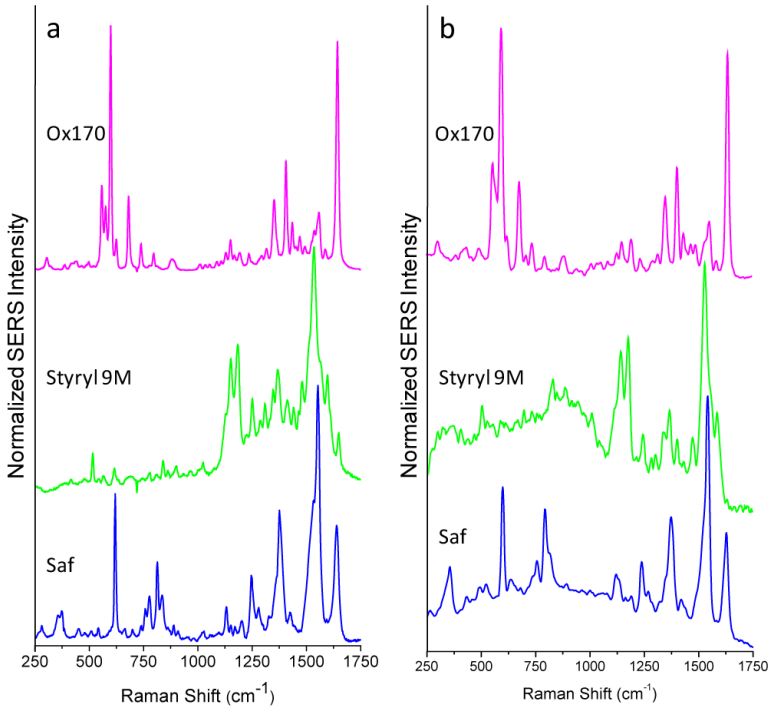

Figure 2.

(a) Bulk spectra of oxazine 170 (Ox170), styryl 9M and safranine (Saf) SERS-tags taken with 0.5 mW of 514 nm or 488 nm (safranine only) excitation, 10 s integration times. (b) Analogous spectra taken in flow on a single SERS-tag particle with 50 mW of 514 nm or 488 nm (safranine only) excitation, 20 μs integration times.

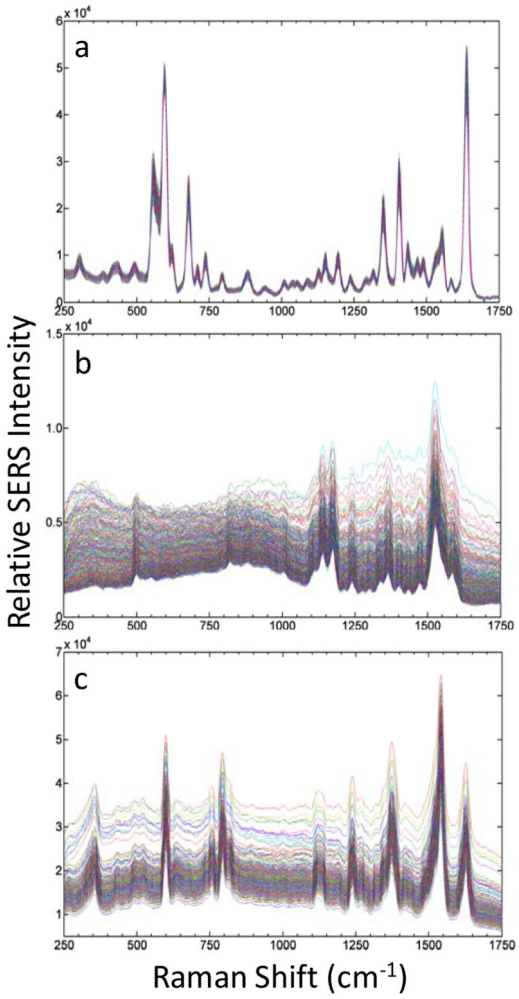

Figure 3.
Plot of spectra from 1000 single SERS-tags, taken with 50 mW of 514 nm excitation from: (a) Oxazine 170 tags; (b) Styryl 9M tags; (c) safranine tags (with 50 mW of 488 nm excitation). Integration time of 20 μs for each spectrum. A background spectrum from PBS has been subtracted from each single-tag spectrum.

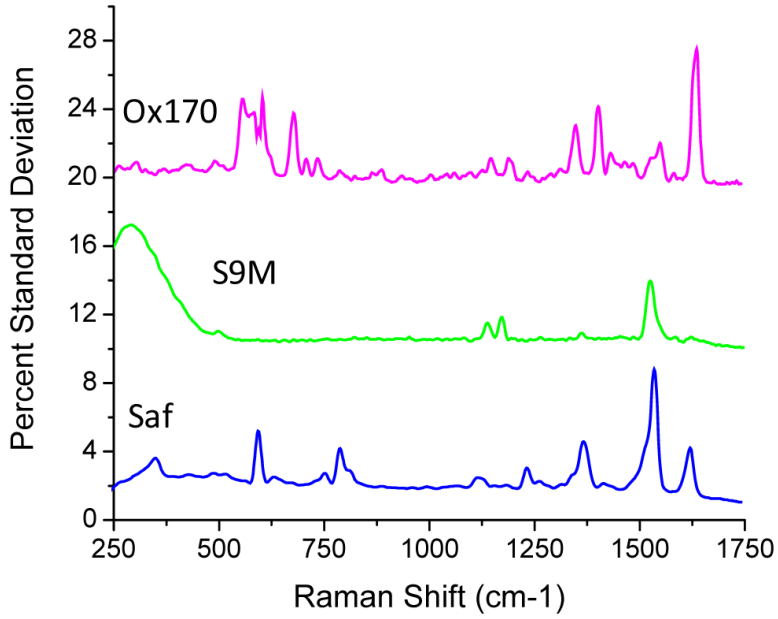

Figure 4.
Pixel-by-pixel percent standard deviations of particle spectral variability for each of the three SERS-tag populations of Figure 3. Plots are offset for clarity.

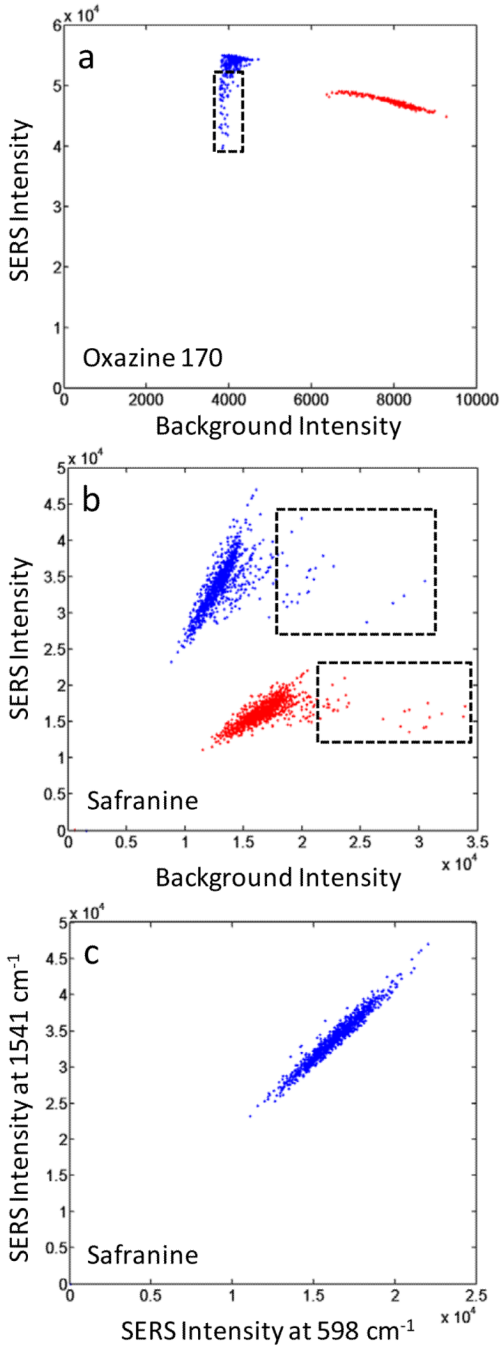

Figure 5.

Correlated Raman intensities at different frequencies for 1000 individual SERS-tag particles. (a) Oxazine 170, 1638 cm^{-1} peak compared to 1706 cm^{-1} background (blue) and 595 cm^{-1} peak compared to 642 cm^{-1} background (red); (b) Safranine, 1541 cm^{-1} peak compared to 1583 cm^{-1} background (blue) and 598 cm^{-1} peak compared to 534 cm^{-1} background (red); (c) Safranine, 1541 cm^{-1} peak compared to 598 cm^{-1} peak. Small subpopulations in behavior are highlighted by the dashed rectangles. Peak intensities are background-subtracted. Data extracted from the spectra of Figures 3a and 3c.

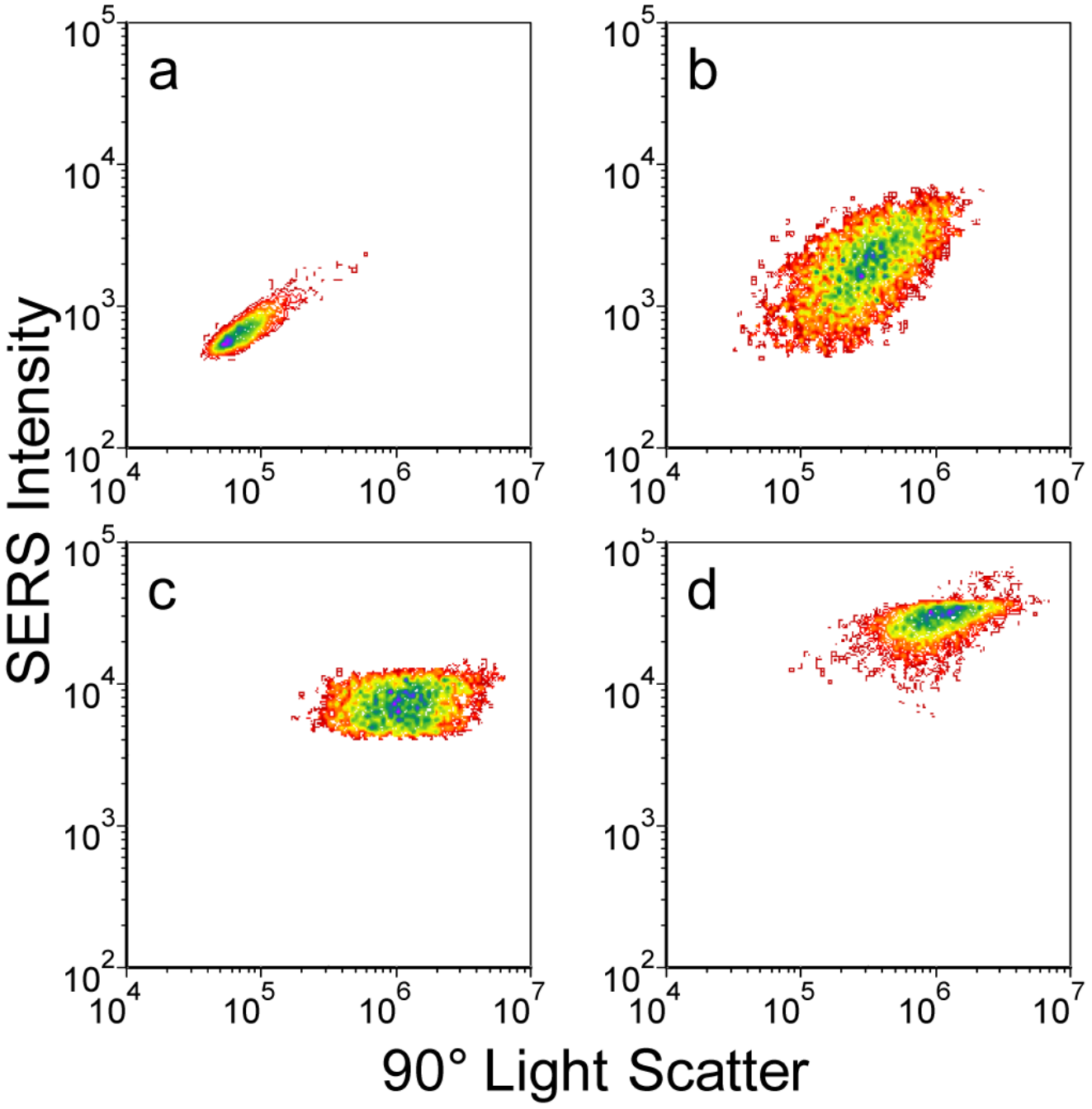

Figure 6.
Bivariate histograms of (a) ~100 nm beads and (b–d) silver nanoparticle aggregates. Each histogram represents roughly 10,000 individual particles. Color contours represent particle counts, with red corresponding to fewer/individual particles and blue corresponding to greatest number of particles. (a) 100 nm fluorescent microspheres. (b) Oxazine 170. (c) Styryl 9M. (d) Safranine. Samples were interrogated at 532 nm, with 1 mW of power, and 250 μs integration time per particle.

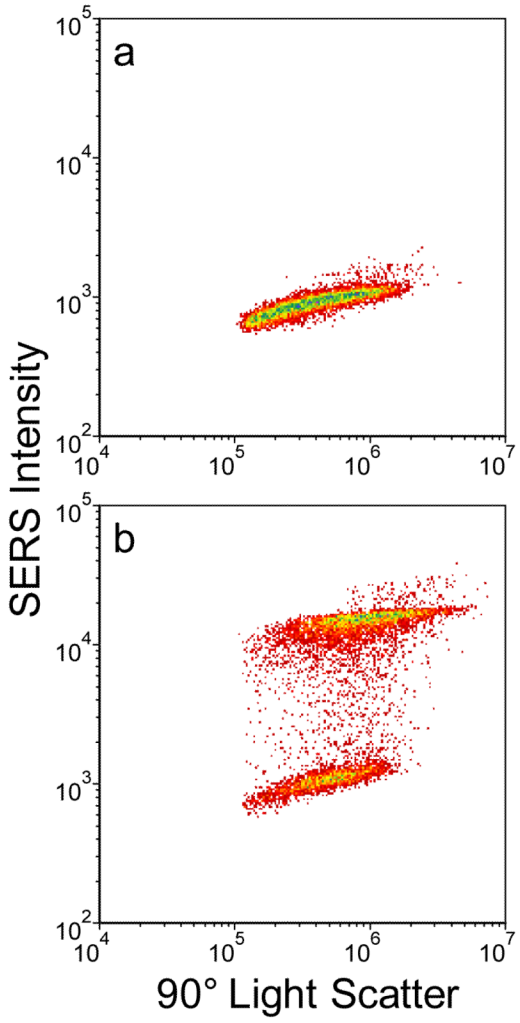

Figure 7.
Bivariate histogram of approximately 10,000, 100 nm silver nanoparticle aggregates from independent preparations. Color contours represent particle counts as per Figure 6. (a) Unconjugated. (b) With Safranine dye attached to surface of nanoparticle. Excitation with 1 mW at 532 nm, 250 μs integration time per particle.

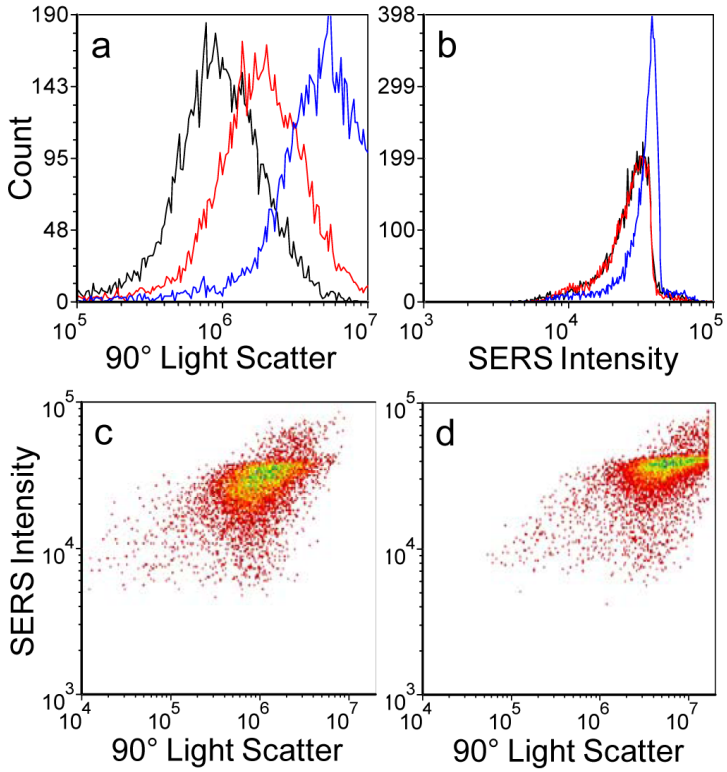

Figure 8.

Univariate histograms of: (a) Side scatter intensity; and (b) SERS intensity for approximately 8,000 safranine-labeled SERS-tags as a function of three different laser power levels: 1 mW (black), 1.5 mW (red), 3 mW (blue). For comparison, bivariate histograms for the same particle sets showing light scatter versus Raman signal for: (c) 1 mW laser power; (d) 3 mW laser power. Excitation at 532 nm, 250 μs integration time per particle. Color contours represent particle counts as per Figure 6.